ENVIRONMENTAL RESEARCH
CLIMATE

PURPOSE-LED PUBLISHING™

PAPER • OPEN ACCESS

Influence of large-scale atmospheric circulation and Mediterranean sea surface temperature to extreme land precipitation: the case of storm Alex

To cite this article: Laurent Terray and Margot Bador 2025 *Environ. Res.: Climate* **4** 015002

ENVIRONMENTAL RESEARCH
CLIMATE

OPEN ACCESS

RECEIVED
6 October 2024

REVISED
6 January 2025

ACCEPTED FOR PUBLICATION
14 January 2025

PUBLISHED
24 January 2025

PAPER

Influence of large-scale atmospheric circulation and Mediterranean sea surface temperature to extreme land precipitation: the case of storm Alex

Laurent Terray* and **Margot Bador**

CECI CNRS/Cerfacs, Université de Toulouse, Toulouse, France
* Author to whom any correspondence should be addressed.

E-mail: terray@cerfacs.fr

Keywords: extreme precipitation, storm Alex, dynamical adjustment, Clausius–Clapeyron scaling

Supplementary material for this article is available online

Abstract

Extreme (greater than 500 mm) amount of rain fell in southeastern France and northern Italy on 2nd and 3rd October 2020 during a 'Mediterranean episode' triggered by the powerful extratropical cyclone Alex. Here we use a dynamical adjustment methodology based on constructed analogues to assess the contributions of different drivers to the magnitude of this extreme precipitation event. We first show that the mean effect of the observed atmospheric circulation pattern, an intense low-pressure system centered over the coasts of Western Europe associated with a cold pool and a secondary low-pressure system, can explain about 80% of the precipitation event magnitude. By contrasting the effect of Alex atmospheric circulation with an anomalously warm Mediterranean sea and eastern Atlantic ocean versus neutral sea surface temperature (SST) conditions, we show that the influence of September 2020 positive SST anomalies can explain a large fraction of the 20% residual precipitation over southeastern France and northern Italy. Finally, based on a storyline approach, we find that the dynamic component, the atmospheric circulation contribution to the extreme precipitation event, was more extreme than it would have been, had it occurred during the mid-20th century. The increase in the magnitude of the dynamic component since 1950 follows a Clausius–Clapeyron scaling, in agreement with previous studies about the intensity changes of Mediterranean extreme precipitation episodes. (limit = 300 words).

1. Introduction

In early October 2020, the extratropical Storm Alex emerged as a meteorological phenomenon of extreme magnitude, leaving an indelible mark on southeastern France and northern Italy. This meteorological event, characterized by its unusual intensity and prolonged duration, unleashed a sequence of heavy precipitation and flash floods that had far-reaching consequences for the natural environment, infrastructure, and communities across the Southern Alps. This extreme precipitation event led to unprecedented precipitation totals in the Roya, Vésubie and Tinée valleys of the Alpes Maritimes district located in southeastern France. From 6 a.m on 2nd October to 6 a.m on 3rd October, the Lac des Mesches (in the Roya valley) and Saint-Martin Vésubie rain gauges recorded 663 and 576 mm of precipitation, respectively (Chochon *et al* 2021). Extreme amounts of precipitation were also recorded in the Italian Piemonte (630 mm at Sambughetto and 580 mm at Limone Piemonte on 3rd October). This precipitation event is characteristic of *Mediterranean episodes*, a class of extreme heavy precipitation events (HPEs) that occur around Mediterranean coastal regions, in particular in the south of France during the extended fall season typically from September to December (Nuissier *et al* 2008, Ducrocq *et al* 2014). HPEs are typically of short duration (a few hours up to a couple of days) and their magnitude often exceeds 100 mm within a few hours. These HPEs are the result of favorable dynamical (fast upper troposphere wind, a warm and moist marine low-level jet, and mesoscale lifting due to orographic barrier and/or surface wind convergence) and thermodynamic

(conditionally unstable atmosphere) factors (Dayan *et al* 2015). Previous studies have found an increasing trend in Mediterranean HPE intensity and frequency during the last decades (Blanchet *et al* 2018, Ribes *et al* 2019).

Based on an analogue-based approach, Ginesta *et al* (2023) suggested that the characteristics of Alex-like extratropical storms have also changed since 1950; a warmer climate leads to enhanced persistence of atmospheric patterns and more energetic storms (stronger turbulent kinetic energy maximum during storm growth and lower pressures during decay). These storminess changes can favor more extreme precipitation events associated with Alex-like extratropical storms. One of the other possible factors in the past and future amplification of Mediterranean HPE intensity is the influence of Mediterranean sea surface temperature (SST). Early studies based on numerical simulations have shown that mean SSTs in the upstream neighborhood of the precipitation event control the total amount of rain (Pastor *et al* 2001, De Zolt *et al* 2006, Lebeaupin *et al* 2006). The simple physical argument is that a warm (cold) sea surface moistens and heats up the marine boundary layer, which then becomes more unstable and can trigger larger (smaller) amounts of rainfall. However, the story is not so simple because a warm sea surface can also accelerate the low-level jet and lead to convective systems that are less quasi-stationary, thereby reducing the total amount of rainfall (Stocchi and Davolio 2016, Meroni *et al* 2018).

On the other hand, several numerical studies have also shown that the fine-scale structure of Mediterranean SST patterns can lead to changes in the location of the HPE rain bands while leaving the total amount of rainfall relatively unchanged (Lebeaupin Brossier *et al* 2013, Berthou *et al* 2015). Here, the main mechanism is that the sub-mesoscale SST horizontal gradients impact the SST-wind relationship through the spatial structure of the surface wind convergence and the downward momentum mixing mechanism, thereby displacing the oceanic HPE rain bands (Meroni *et al* 2018).

This paper seeks to comprehensively examine and quantify the main drivers of the extreme HPE that led to highly destructive flash floods in the Southern Alps during the critical period from 2nd October to 3rd October, 2020. We use the classical dynamic and thermodynamic framework to disentangle the roles of different factors contributing to the early October 2020 Mediterranean HPE. Based on the dynamical adjustment methodology, we first perform a conditional analysis of the extreme precipitation event with regard to the large-scale atmospheric circulation. We first quantify the contribution of the intense low-pressure system and associated strong, warm and moist low-level jet to the total amount of precipitation recorded over a geographical domain that includes the french Alpes Maritimes and the Italian Piemonte (see figure S1 for the geographical location of these two regions and the domain). We then investigate whether the warm Mediterranean Sea surface observed in September 2020 has contributed to the inflow of moisture and therefore to the extreme precipitation amounts. Finally we discuss the potential role and contribution of anthropogenic climate change to the extreme HPE magnitude.

2. Data and methods

We first present the reanalysis and observed datasets before giving a brief summary of the dynamical adjustment methodology.

2.1. Data

We use the ERA5 reanalysis as our main dataset (Hersbach *et al* 2020, 2023). The atmospheric circulation variable used as a predictor in dynamical adjustment is the daily sea level pressure and the characterization of the extreme precipitation event is based on the daily precipitation. When computing spatially-averaged precipitation amounts, we only consider land precipitation and define land grid points as grid points having a land fraction greater than 25% (in order to account for coastal grid points). We also make use of ERA5 SSTs and 2 m air temperature products. We use the full 1940–2023 period for the dynamical adjustment of the event based on ERA5. Anomalies when shown are estimated relative to the 1991–2020 period. We note that the evaluation of ERA5 precipitation relative to station data suggests that ERA5 can be used for extratropical precipitation monitoring (Lavers *et al* 2022). Regarding extreme events, it is known that ERA5 cannot model the highest event magnitude (figure 1) but that it is often able to accurately capture the spatial patterns, intensity distribution and the temporal consistency of extreme precipitation events (Rivoire *et al* 2021).

We also use the high-resolution observed COmbinaison en vue de la Meilleure Estimation de la Précipitation HOraiRE (COMEPHORE) dataset, a precipitation blended product produced by Météo France using all available *in situ* and radar rainfall records (Champeaux *et al* 2009, Tabary *et al* 2012, Caillaud 2019, Fumière *et al* 2020). The COMEPHORE product covers the 1997–2022 period at hourly frequency and 1 km spatial resolution. Note that the COMEPHORE geographic domain is limited to France.

The rainfall analysis focuses on a geographical domain (see the magenta box region in figure S1) that includes both the Alpes Maritimes, the Italian Piemonte and the northern Italy-Switzerland border. Heavy

precipitation for the French side occurred mostly on 2nd October while it rained heavily on the Italian and Swiss side during the whole period (2nd–3rd October). In the following, we define the magnitude of the HPE by the amount of accumulated 2 d rainfall, spatially averaged over the whole area of the above geographical domain.

2.2. Dynamical adjustment

Dynamical adjustment aims to identify the causal factors that lead to a given extreme event with an approach conditional on the observed large-scale atmospheric circulation during the event. Our dynamical adjustment approach is based on the constructed analogue method (Van den Dool *et al* 2003) and used to identify the *mean* large-scale atmospheric circulation contribution to the extreme precipitation associated with storm Alex. Here *mean* means averaging over many different ocean and land surface conditions (see below).

We use sea level pressure as our large-scale atmospheric circulation variable. We use the domain 35°–70° N, 25° W–30° E for the sea level pressure patterns. First, we reconstruct the sea level pressure spatial pattern for a given extreme precipitation day using an optimal linear combination of daily sea level pressure patterns (equations (1) and (2)). The number of patterns is typically on the order of a few hundreds depending on the size of the geographical domain (here we use 300 patterns). The patterns are randomly selected from a pre-defined library of sea level pressure patterns. The library contains all daily sea level pressure patterns in a time window (here $\pm$15 days centered on the extreme precipitation day) from all ERA5 years (1940–2023 but excluding the year of the event, here 2020). This means that the library contains 83 (number of ERA5 years minus one) x31 (number of days in the time window) = 2573 daily sea level pressure patterns.

One can then write:

$$\boldsymbol{X}_{\mathrm{hpe}} \approx \boldsymbol{X}_{\mathrm{ca}} = \boldsymbol{X}_i \boldsymbol{\beta} \tag{1}$$

where $\boldsymbol{X}_{\mathrm{hpe}}$ is a column vector representing the sea level pressure on the day of the extreme event, $\boldsymbol{X}_i$ is a matrix of column vectors comprising the 300 selected sea level pressure patterns, $\boldsymbol{X}_{\mathrm{ca}}$ is a constructed sea level pressure analogue of $\boldsymbol{X}_{\mathrm{hpe}}$ based on an optimal linear combination of the $\boldsymbol{X}_i$, and $\boldsymbol{\beta}$ is a column vector of the fitted regression coefficients that are the linear proportions of the contributions of each column of $\boldsymbol{X}_i$ to the constructed analogue $\boldsymbol{X}_{\mathrm{ca}}$. The dimensions of $\boldsymbol{X}_{\mathrm{hpe}}$ and $\boldsymbol{X}_{\mathrm{ca}}$ are $m \times 1$, where m is the number of grid points contained in the sea level pressure pattern. The dimensions of $\boldsymbol{X}_i$ are $m \times 300$ and that of $\boldsymbol{\beta}$ are 300×1. The $\boldsymbol{\beta}$ coefficients can be estimated by using the Moore–Penrose pseudoinverse of $\boldsymbol{X}_i$:

$$\boldsymbol{\beta} = \left[\left(\boldsymbol{X}_i^{\mathrm{T}} \boldsymbol{X}_i \right)^{-1} \boldsymbol{X}_i^{\mathrm{T}} \right] \boldsymbol{X}_{\mathrm{hpe}}. \tag{2}$$

In practice, we estimate the $\boldsymbol{\beta}$ coefficients based on a singular value decomposition of the $\boldsymbol{X}_i$. The $\boldsymbol{\beta}$ coefficients are then applied to the 300 daily precipitation patterns $\boldsymbol{Y}_i$ corresponding to the 300 daily sea level pressure patterns $\boldsymbol{X}_i$ to derive a first estimate of the large-scale circulation-related component of precipitation $\boldsymbol{Y}_{\mathrm{rec}}$. These steps (random selection of sea level pressure patterns, optimal reconstruction of the constructed analog and application of the $\boldsymbol{\beta}$ coefficients to the precipitation patterns) are then repeated many times (here we use 200 iterations) in order to sample many different land and ocean states that might otherwise influence the estimate of the precipitation dynamically induced component. Finally, for each extreme precipitation day, the 200 reconstructed precipitation spatial maps are averaged together (equation (3)), providing the 'mean estimate' $\boldsymbol{Y}_{\mathrm{dyn}}$ of the precipitation dynamically induced component (the precipitation dynamic component thereafter):

$$\boldsymbol{Y}_{\mathrm{dyn}} = \frac{1}{200} \sum_{j=1}^{200} \boldsymbol{Y}_{\mathrm{rec}}^{j}. \tag{3}$$

The precipitation dynamical component $\boldsymbol{Y}_{\mathrm{dyn}}$ can then be subtracted from the raw precipitation $\boldsymbol{Y}_{\mathrm{hpe}}$ to get a residual component $\boldsymbol{Y}_{\mathrm{res}}$. This residual includes the potential effect of land and ocean surface anomalies (such as soil moisture or SST anomalies) on the magnitude of the precipitation event, in addition to the potential contribution of small-scale atmospheric circulation systems such as mesoscale convective systems and the possible precipitation response to anthropogenic forcing.

In practice, we estimate $\boldsymbol{Y}_{\mathrm{dyn}}$ and a 95% confidence interval based on bootstrapping. Bootstrapping makes no apriori assumption about the distribution of the $\boldsymbol{Y}_{\mathrm{rec}}$ samples and is adapted to small sample size datasets. We randomly draw (with replacement) 200 $\boldsymbol{Y}_{\mathrm{rec}}$ samples a 1000 times to produce a distribution of bootstrapped samples that can then be used to derive a bootstrapped mean and a 95% confidence interval given by the bootstrapped low (2.5%) and high (97.5%) percentile values. Furthermore, the distribution of

bootstrapped samples can be used to derive similar statistical properties for $\boldsymbol{Y}_{\text{res}}$ (simply because $\boldsymbol{Y}_{\text{res}} = \boldsymbol{Y}_{\text{hpe}} - \boldsymbol{Y}_{\text{dyn}}$)or any scalar values involving an area-averaged of the dynamic or residual component. We refer to Terray (2021, 2023) for an additional description of the method and its application to extreme event attribution.

3. Results

Figure 1 shows how the extreme HPE unfolded during the 2nd–3rd October period in the ERA5 reanalysis. On 2nd October early morning, the Alex low-pressure center is initially located north of Britany. It then moves slowly southward to reach the Atlantic coast before moving inland eastward during the early morning of 3rd October.

Heavy precipitation is initially located in the southern United Kingdom and across France from the southwest up to the northern boundary. With a southerly to southwesterly flow at all levels, heavy rain began to fall along the French eastern Mediterranean coast on October 2nd around 06:00 UTC, before settling inland for 9 up to 12 h. During this phase, the strong east-west pressure gradient and the north–south orientation of the Alpes Maritimes and Italian valleys favored the advection of warm and moist low-level jet and extreme precipitation, further enhanced by orographic lifting. The combination of high intensity and unusual duration made the total amount of precipitation truly exceptional for the area (Chochon *et al* 2021, Kreitz 2021). At the end of the period (the first 6 h of 3rd October), the atmospheric flow turned eastward leading to a shift and increase of intense convection towards Italy. This effect is enhanced by the formation of a secondary low-pressure center over the Piemonte region that leads to the persistence of intense precipitation across the northern Italian Alps during the whole 3rd October day.

Figure 1(k) also shows that the high-resolution observed precipitation amount in France reaches its maximum at 12:00 UTC on 2nd October with values up to 86 mm per hour in the Alpes Maritimes valleys. As expected, low resolution ERA5 values are much lower and the peak of precipitation rate in ERA5 occurs in 2nd October late afternoon. As the COMEPHORE dataset does not include the Piemonte region and only covers the 1997–2022 period, we prefer using ERA5 as our main dataset for this study.

In the following, we only use ERA5 precipitation data and focus on the HPE magnitude as previously defined. We acknowledge that, given the ERA5 spatial resolution (∼30 km), we are not resolving small scale features that are important to fully represent the distribution and local features of extreme precipitation in this complex mountainous region.

3.1. Atmospheric circulation contribution to the extreme precipitation event

We now assess the contribution of Alex low-pressure synoptic pattern to the magnitude of the extreme HPE. We focus our analysis on the broad region that includes both southeastern France and the Italian Piemonte (magenta box in figure 2). We perform dynamical adjustment of the 2 day period (2nd–3rd October) based on ERA5 sea level pressure and precipitation daily data from the 84 yr period (1940–2023).

Figure 2 shows that the daily sea level pressure is accurately reconstructed by the dynamical adjustment based on constructed analogues. The dynamic component explains a large fraction of the total amount of precipitation for the 2 days and the whole period (figures 2(b), (e) and (h)). The dynamic component contribution explains 81 $\pm$ 4% (95% confidence interval) of the HPE magnitude (75% and 92% for 2nd and 3rd October, respectively). Consequently, the residual component has a much stronger magnitude for 2nd October than 3rd October , suggesting that an additional factor had a much larger contribution during the HPE initial phase than the final one, in particular in the Southern French Alps. On 2nd October the amount of precipitation and both dynamic and residual component contributions are large over both the Alpes Maritimes and the Piemonte regions. In contrast, the intense precipitation shifts eastward and is mainly observed the Piemonte and the northern and eastern Italian and Swiss Alps on 3rd October. The dynamic component also represents a large fraction of the HPE magnitude over northwestern Spain and the Pyrénées.

3.2. Warm Mediterranean Sea contribution to the extreme precipitation event

September 2020 was characterized by positive SST anomalies over a large fraction of the Western Mediterranean Sea (figure 3). We investigate whether these positive SST anomalies have contributed to the extreme magnitude of the event based on two additional dynamical adjustments.

The dynamical adjustment algorithm is exactly the same as the one we have used in section 3.1, with the only difference being the construction of the daily sea level pressure pattern library in the two additional dynamical adjustments.

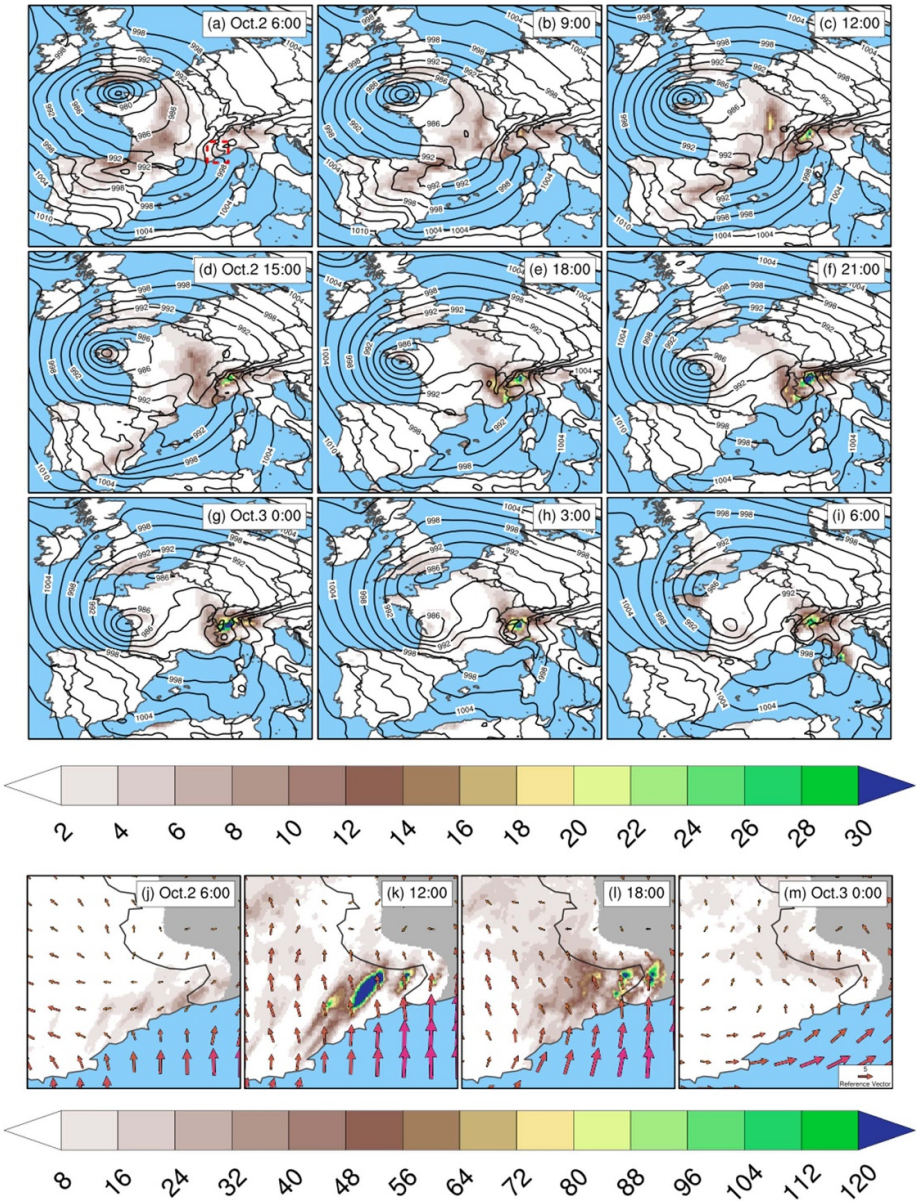

Figure 1. ERA5 hourly sea level pressure (contours; hPa) and 3-hourly cumulative precipitation (color shading; mm): (a)–(f) 2nd October at 6:00, 9:00, 12:00, 15:00, 18:00 and 21:00. (g)–(i) 3rd October at 0:00, 3:00 and 6:00. The time indicated in the upper right corner gives the day and the middle hour of the 3-hourly period. Sea level pressure contour interval is 3 hPa. (j)–(m) ERA5 hourly 10 m winds (arrows; $m{\cdot}s^{-1}$) and COMEPHORE 3-hourly cumulative precipitation (color shading; mm) on 2nd October at 6:00, 12:00, 18:00 and 3rd October at 0:00 zoomed in the red box region shown in (a). The reference wind vector in (m) has a magnitude of 5 $m{\cdot}s^{-1}$. Note the different color scales in (a)–(i) and (j)–(m).

In the first one, the goal is to determine the contribution of the Alex low-pressure synoptic pattern to the magnitude of the extreme HPE when the Mediterranean Sea is warm. In other words, we want to condition the dynamical adjustment on the presence of positive Mediterranean SST anomalies. To do so, we first define a broad SST region (blue box region in figures S1 and 3) which includes most of the Western Mediterranean positive SST anomalies in September 2020 (figure 3(a)). We then derive standardized monthly SST indices (for both September and October, with standard deviation σ_{Sep} and σ_{Oct}) representing area-averaged SST over the 1940–2023 period. We then first select October and September months that are characterized by positive Mediterranean SST anomalies (SST index > 1.5, 1.5 being the value of the index for September 2020). The large-scale features of the warm Mediterranean Sea surface composite map are very similar to that of the September 2020 SST anomalies (figures 3(a) and (b)). Both maps show a V-shape pattern going from the southern tip of Sardinia to northern Corsica. Furthermore, both maps show positive SST anomalies along the coasts of Western Europe, from Spain up to northern Germany. This suggests that the occurrence of western Mediterranean positive SST anomalies in early autumn is often associated with a large-scale atmospheric pattern leading to warm sea surface conditions in the Eastern Atlantic. Finally, all daily sea level

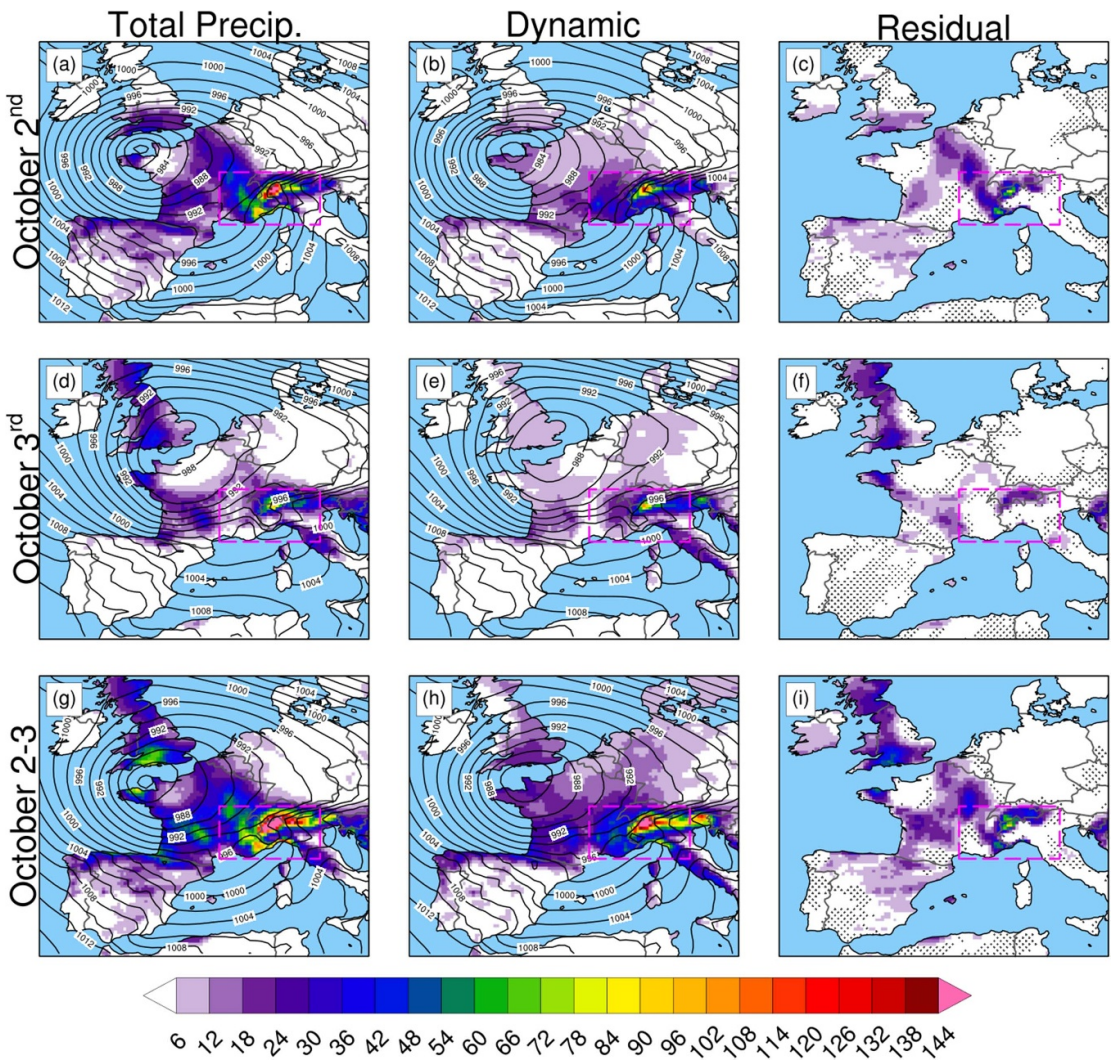

Figure 2. ERA5 daily precipitation (color shading; mm) and daily mean sea level pressure (contours; hPa): (a) 2nd October total precipitation and sea level pressure (b) precipitation dynamic component and reconstructed sea level pressure (c) Precipitation residual component; (d)–(f) same as (a)–(c) for 3rd October; (g)–(i) same as (a)–(c) for the 2nd–3rd October period. Sea level pressure contour interval is 2 hPa. Stippling indicates grid points for which the residual component values are not significantly different from 0 at the 5% level. Note that negative values can be found in the residual in case the dynamic component displays values greater than the observed ones. The magenta box in all panels shows the region used to estimate the HPE magnitude based on the area-averaged precipitation during the 2 d event.

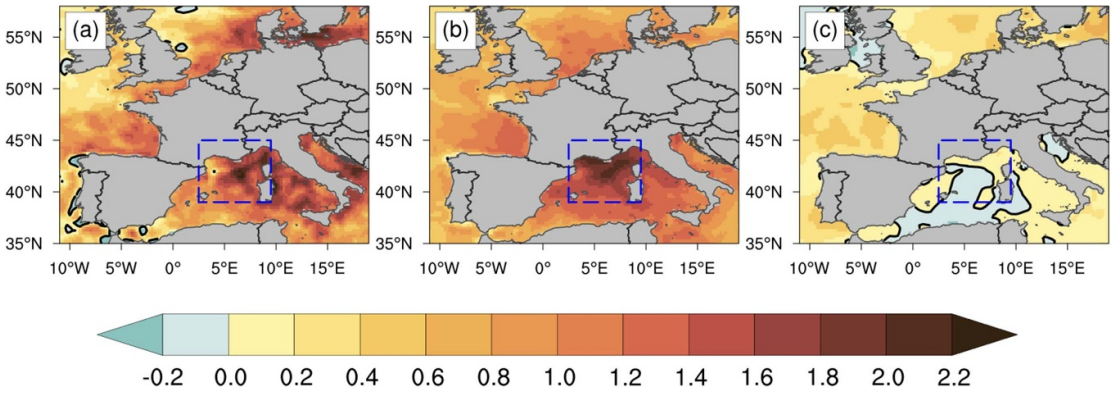

Figure 3. ERA5 sea surface temperature monthly mean anomaly (color shading; °C): (a) September 2020; (b) monthly mean warm SST composite with all September and October months having a standardized SST index—I_{SST}—greater than 1.5 (the SST index is the mean SST averaged over a western Mediterranean region (blue box in (a)–(c)); (c) the same as (b) but for the neutral SST composite (with $|I_{SST}| < 0.1$). Note that September and October I_{SST} values are standardized separately.

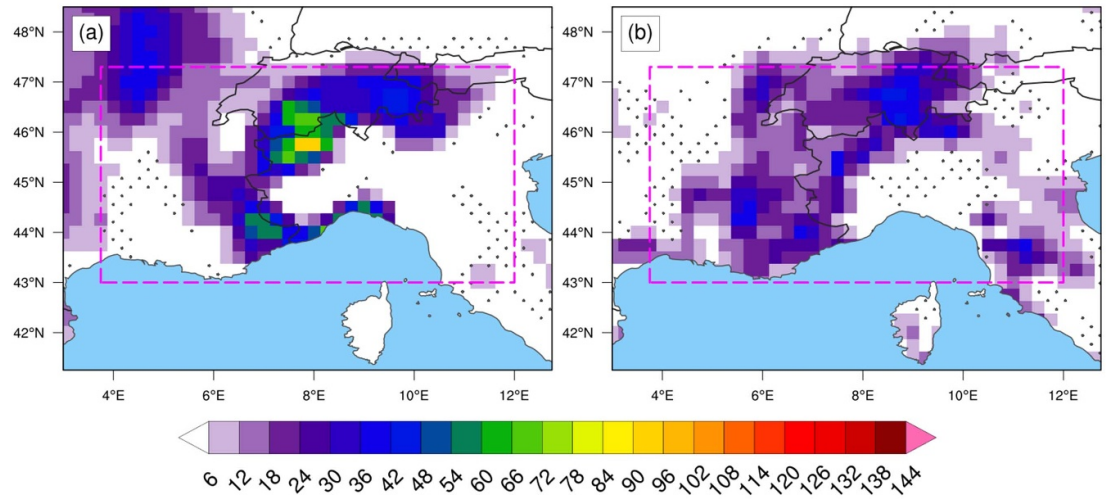

Figure 4. ERA5 total precipitation (color shading; mm) during the 2nd–3rd October period: (a) precipitation residual component (same as figure 2(i) but zoomed in); (b) difference between the precipitation dynamic components coming from the two additional dynamical adjustments (see section 3.2). In (a), stippling indicates grid points where residual component values are not statically different from 0 at the 5% level. In (b), we derive a 95% confidence interval of the difference between the two dynamic components based on bootstrapping. Stippling indicates grid points where the difference between the two dynamic components is not statistically different from 0 at the 5% level. The magenta box shows the region used to estimate the HPE magnitude based on the area-averaged precipitation during the 2 d event.

pressure patterns from the selected September and October months are included in the library that is used to perform the first additional dynamical adjustment.

In the second one, we want to condition the dynamical adjustment on the presence of neutral Mediterranean SST conditions. In this case, the library is defined by including all daily sea level pressure patterns from September and October months characterized by neutral Mediterranean SST conditions (defined by the absolute value of the SST index < 0.1, figure 3(c)). The resulting library is then used to perform the second additional dynamical adjustment.

Taking the difference between the two dynamic components coming from the two additional dynamical adjustments gives an estimate of a warm sea surface contribution to the precipitation residual (resulting from the initial dynamical adjustment based on all September and October days of the 1940–2023 period) and therefore, to the extreme event magnitude.

Figure 4 shows that the presence of warm Mediterranean and eastern Atlantic sea surface leads to enhanced precipitation over the French Alpes Maritimes and Italian Piemonte. The additional precipitation is located along a southwest-northeast track that strongly overlaps with regions with large values of the residual component. To quantify the contribution of positive SST anomalies to the magnitude of residual component (figure 4(a)), we only use grid points having positive values in the residual (meaning that the dynamical component alone cannot fully explain the total precipitation amount for these locations). The whole region-averaged warm sea surface contribution to the residual component magnitude is 62% [49%–75%] (95% confidence interval).

One may ask what is the relative role of Mediterranean versus Atlantic SSTs regarding the contribution of a warm sea surface to the precipitation dynamic component over the French Alpes Maritimes and Italian Piemonte. Dynamical adjustment by itself cannot separate the relative contributions of the two SST regions. In Bador *et al* (2025) and based on a trio of simulations with the kilometer-scale CNRM-AROME regional model (Caillaud *et al* 2021), it is shown that the additional precipitation increase due to positive SST anomalies is mainly due to the Mediterranean SSTs (their figures 9, 12 and 13). The CNRM-AROME simulations also show that eastern Atlantic positive SST anomalies lead to a greater spatial extent and a deepening ($\sim$2 hPa) of the Alex low pressure system but do not seem to significantly influence Mediterranean precipitation during the HPE (Bador *et al* 2025).

3.3. Extreme event magnitude and Clausius–Clapeyron scaling

Previous studies have shown that observed HPE intensity has increased in Mediterranean Southern France over the 1961–2015 period. The best-estimate of annual maximum precipitation change was found to be +22% (with a 90% confidence interval of +7% to +39%) which is roughly twice the Clausius–Clapeyron rate given the observed annual mean warming over that period (Ribes *et al* 2019). Note that the uncertainty range is quite large as the observed change is consistent with 1–3 times the Clausius–Clapeyron scaling. Here

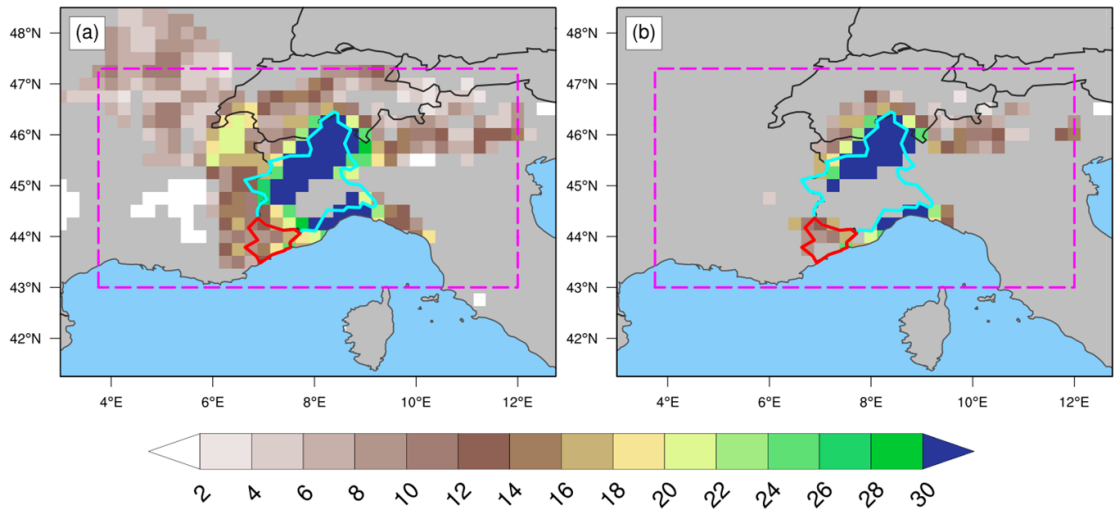

Figure 5. Difference in 2nd–3rd October precipitation dynamic component (color shading; mm) based on ERA5 sea level pressure daily analogues between 1980–2019 and 1940–1979. Grey squares indicates grid points where the total ERA5 precipitation during the HPE is less than: (a) 40 mm (b) 80 mm. The dashed magenta box shows the region used to estimate the magnitude increase of the HPE dynamic component. The red and cyan contours delimitate the Alpes Maritimes and Piemonte regions, respectively.

we use a storyline approach and ask the following *what-if* question: what would be the change in the magnitude of the HPE dynamic component if the HPE had occurred in a period with a much weaker anthropogenic forcing? To answer this question, we first divide the 1940–2019 period in four 20 year sub-periods: 1940–1959, 1960–1979, 1980–1999, and 2000–2019.

We then perform 4 additional dynamical adjustments to the 2020 HPE. Again, the only difference between these 4 additional adjustments and the first one is the definition of the sea level pressure pattern library. For each of the 4 periods, the library includes all daily sea level pressure patterns from the September and October months of the given period.

We end up with 4 different estimates of the dynamic component (figure S2). The spatial patterns of the 4 dynamic components are very similar. However, the magnitude of the HPE dynamic component significantly increases after 1980 over a broad southeastern France and Piemonte region.

We now assess the magnitude change over the 1940–2019 period by comparing the dynamic component between the first (1940–1979) and last (1980–2019) 40 yr periods. Based on resampling with replacement, we first generate a 1000 estimates of the average of the 1940–1959 and 1960–1979 dynamic components. We then use the mean of the 1000 bootstrapped estimates as our best-estimate of the 1940–1979 dynamic component. The same approach is used for the 1980–2019 dynamic component based on the appropriate 20 yr dynamic components. As we are interested in the scaling of extreme precipitation values with temperature, we first select the area where the ERA5 total precipitation (cumulated over the 2 d) is greater than a given fixed threshold. We then apply the resulting spatial mask to the 1980–2019 and 1940–1979 HPE dynamic components and estimate their magnitude for each 40 yr period (by area averaging non-missing precipitation values within the magenta box in figure 5). Figure 5 shows the difference between the two dynamic components with a spatial mask given by the 40 and 80 mm precipitation thresholds (these two values straddle the 60 mm classical fixed threshold often used to characterize extreme precipitation events in the Mediterranean region, see Jansa *et al* 2014).

Normalizing the HPE magnitude difference by the magnitude of the 1940–1979 dynamic component, we can derive the fractional increase in the magnitude of the HPE dynamic component. We find that the magnitude of the HPE dynamic component has seen a ∼11% increase going from the 1940–1979 period to the 1980–2019 period. Changes in magnitude are 10.7 [8.6–12.8], 11.3 [9.4–13.5], 11.1 [9.1–13.2], 11.2 [9.4–13.3] % for the 40, 60, 80, 100 mm thresholds, respectively (the change is given by the mean of 1000 bootstraped estimates based on sampling with replacement and the numbers in brackets are the 2.5 and 97.5% percentiles of the bootstraped estimates). The HPE magnitude increase and its confidence interval show little sensitivity to the precipitation threshold. In the following, we simply use the average of the magnitude increase of the 4 precipitation thresholds (11.1%) as a mean estimate of the magnitude increase and a conservative confidence interval given by the minimum and maximum values ([8.6–13.5]) from the 4 confidence intervals.

We then derive the HPE dynamic component scaling with temperature by combining the change of the HPE magnitude with the observed Autumn (September–October) regional temperature change over the

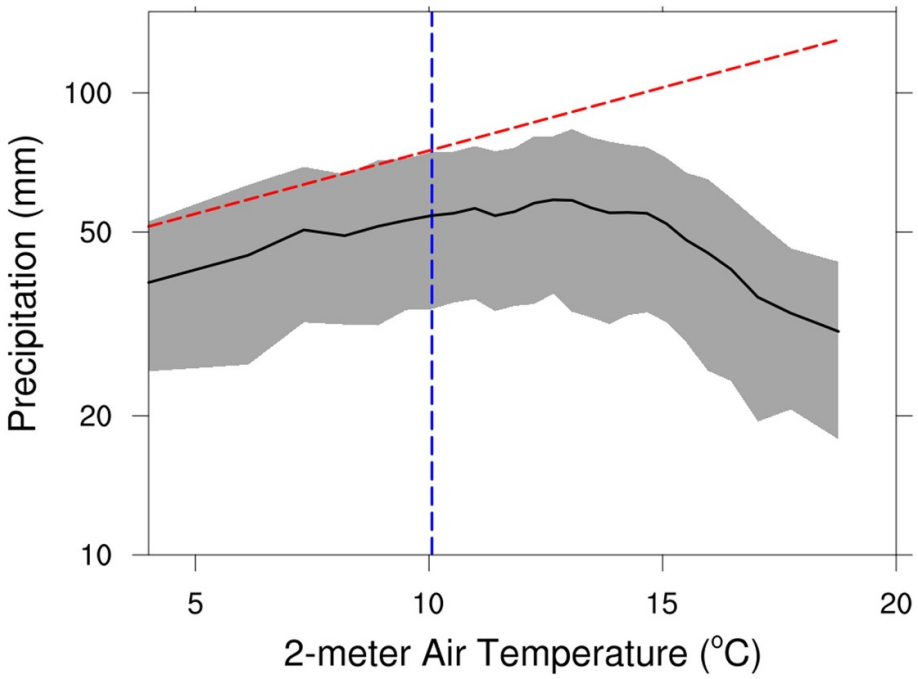

Figure 6. Autumn (SO) daily precipitation extremes (99th percentile, in mm) versus daily averaged temperature (in °C) at all selected land grid points of the HPE region. The thick black line shows the average over all grid points and the grey shading shows the spatial variability around the mean given by ± one standard deviation across all grid points. The red dashed line indicates the Clausius–Clapeyron slope using the August–Roche–Magnus approximation for saturated vapor pressure at 15 °C. The blue dashed line gives the temperature during the HPE (averaged over the 2nd–3rd October period and spatially averaged over the area with HPE total precipitation greater than 40 mm, meaning over all non-missing grid points in figure 5(a)). A log-scale is used for the *Y*-axis.

1940–2023 period. We estimate a regional warming of +1.4 K based on the application of a low-frequency Loess filter with a smoother length of 45 years (figure S3). Based on a magnitude change of 11.1 [8.6–13.5] %, this leads to an HPE scaling of ∼+7.9 [6.1–9.6]% °C^{-1} to be compared with the theoretical Clausius–Clapeyron scaling of +6.5% °C^{-1} (at a temperature of 15 °C). The dynamical adjustment results then suggest that the change in the magnitude of the HPE dynamic component is consistent with the Clausius–Clapeyron rate and close to the lower bound but still within the scaling range from Ribes *et al* (2019).

The HPE dynamic component scaling with temperature is also consistent with the *observed* Clausius–Clapeyron scaling (Drobinski *et al* 2018). Following Drobinski *et al* (2018), all (within the 1940–2023 period) Autumn (September–October) daily precipitation–temperature pairs from a given gridpoint within our region of interest (the magenta box in figure 5) are placed in temperature bins according to increasing temperature, with an equal number of daily samples in each bin (200 samples) and therefore different temperature ranges for each bin. The mean temperature of the days in each bin is used as the representative temperature for that bin. Within each bin, precipitation intensities are ranked to determine the 99th percentile, taken as representative of extreme precipitation. For a given grid point, we end up with 25 (the number of bins) pairs of temperature-extreme precipitation that shows the scaling of extreme precipitation magnitude with increasing temperature. We then perform the same analysis for all grid points within our region of interest. Figure 6 shows that the *observed* extreme precipitation scaling exhibits the classical hook shape (Drobinski *et al* 2016). We note that the *observed* scaling is close to the Clausius–Clapeyron scaling for temperatures below ∼13 °C and exhibits sub-Clausius–Clapeyron scaling above it (due to the use of 2 m air temperature for a proxy of the temperature at condensation level, see Drobinski *et al* 2016 for details). The temperature during the HPE event (∼10 °C) is below the 13 °C threshold and in the temperature range where the extreme precipitation-temperature relationship follows the Clausius–Clapeyron scaling. We conclude that the HPE dynamic component scaling is also consistent with the *observed* scaling curve and exhibits near-Clausius–Clapeyron scaling.

4. Summary and discussion

Based on the ERA5 reanalysis and making use of a dynamical adjustment approach based on constructed analogues, we have provided insight into the main factors that have contributed to the extreme magnitude of the Mediterranean high precipitation event that occurred during the storm Alex in early October 2020 over southeastern France and northern Italy. Our results show that the main factor (about 80%) of the total magnitude of the extreme event is the large-scale atmospheric circulation pattern over the Mediterranean region associated with an intense, warm and moist south to southwesterly flow near the surface and in the lower troposphere.

Additional applications of the dynamical adjustment approach based on selected days corresponding to either an anomalously warm or near-normal Mediterranean Sea surface, suggest that the residual contribution to the extreme event magnitude can be explained to a large extent (two-thirds) by anomalously warm sea surface conditions in the Western Mediterranean. This is qualitatively consistent with results from Meredith *et al* (2015) who show that a warm Black Sea surface was an important driver of the 2012 Krymsk extreme precipitation event. We hypothesize that the much larger impact of SSTs in the Krymsk case (see their figures 3 and 4(a)) comes from the mostly convective nature of the precipitation event while in the Alex case, we have shown that the dominant driver is the large-scale atmospheric circulation.

Finally, we use a storyline approach to ask what would have been the extreme event magnitude, had it occurred in the middle of the 20th century. Based on different dynamical adjustment runs for four consecutive 20 yr periods, we estimate that the magnitude of the dynamic component of the extreme precipitation event has increased at a rate of $+7.9$ [6.1–9.6]% $°C^{-1}$, which is consistent with the Clausius–Clapeyron scaling. This result is consistent with previous studies focusing on the Mediterranean region (Ribes *et al* 2019) and with the *observed* regional and seasonal scaling as defined in Drobinski *et al* (2016).

Interestingly, our results suggest a much larger contribution from the large-scale atmospheric circulation than the one depicted in Ginesta *et al* (2023) (their figures 7(a)–(d)). This is mainly due to methodological differences. Ginesta *et al* (2023) use the standard analogue method where they consider a class (they use the best 30 analogues) of daily atmospheric circulation patterns that are close (in term of Euclidean distance or other distance metrics) to the atmospheric circulation during the extreme precipitation event. Their estimate of the large-scale atmospheric contribution to any variable of interest (here the precipitation) is then simply the average of the 30 daily maps corresponding to the best-analogue dates. Given the sample size of the ERA5 dataset, even the best analogues are not necessarily very good analogues, meaning that they can display substantial differences in terms of regional circulation features and associated precipitation. These two facts (averaging over the 30 best-analogues and the quality of the analogues) explain the difference with our results in the magnitude of the large-scale atmospheric circulation contribution to the extreme precipitation event. In summary, the main difference between the two approaches is the fact that dynamical adjustment reconstructs almost perfectly the atmospheric circulation during the event while the standard analogue approach considers an average of the closest circulation analogues to the event atmospheric circulation pattern. Finally, and despite the different approaches and definitions of factual (recent) and counterfactual (early) periods, there is a qualitative agreement about the pattern (and to a lesser extent magnitude) of precipitation increase due to the large-scale atmospheric circulation between the two periods (compare figure 5 with their figure 7(d)).

The methodological framework proposed in this study provides a purely data-driven (based on observations and/or reanalyzes only) general template for improving attribution to physical causes and interpretation of observed precipitation extremes in Europe and elsewhere. Application to other seasons, regions, time periods, and parameters will be pursued in future work.

Data availability statement

The ERA5 data that support the findings of this study are openly available at the following URL: https://cds.climate.copernicus.eu/datasets/reanalysis-era5-single-levels?tab=overview and the doi to cite is: Hersbach H, Bell B, Berrisford P, Biavati G, Horányi A, Muñoz Sabater J, Nicolas J, Peubey C, Radu R, Rozum I, Schepers D, Simmons A, Soci C, Dee D, Thépaut J-N (2023): ERA5 hourly data on single levels from 1940 to present. Copernicus Climate Change Service (C3S) Climate Data Store (CDS), DOI: https://doi.org/10.24381/cds.adbb2d47.

The COMEPHORE data are openly available here: https://radarsmf.aeris-data.fr/ and the doi to cite is: Caillaud Cécile (2019) METEO-FRANCE, RADAR COMEPHORE Hourly Precipitation Amount Composite. [dataset]. Aeris. https://doi.org/10.25326/360.

The dynamical adjusment code is available here: https://doi.org/10.5281/zenodo.5584777. All figures were made with the NCAR Command Language (NCL) version 6.6.2 (http://dx.doi.org/10.5065/D6WD3XH5).

Acknowledgment

The authors thank Météo-France for providing the COMEPHORE dataset through the SEDOO data portal (www.sedoo.fr/). The authors thank Dr Julien Boé for stimulating discussion and Dr Laure Coquart for the ERA5 data transfer support. This project has received funding from the European Union's Horizon 2020 research and innovation programme under the Marie Sklodowska-Curie Grant Agreement No 101027577. Last but not least, the authors thank the two anonymous reviewers for their insightful and constructive comments that improved the quality of the manuscript and the *Environmental Research: Climate* editor-in-chief, Noah Diffenbaugh, and his team for the careful and efficient handling of the whole review process.

ORCID iDs

Laurent Terray https://orcid.org/0000-0001-5512-7074
Margot Bador https://orcid.org/0000-0003-3976-6946

References

Bador M, Boé J, Caillaud C, Terray L, Moine M P and Alias A 2025 Mediterranean extreme precipitation: amplification by warmer sea surface temperatures in a kilometer-scale regional model *Clim. Dyn.* (available at: https://hal.science/hal-04417064)

Berthou S, Mailler S, Drobinski P, Arsouze T, Bastin S, Béranger K and Lebeaupin-Brossier C 2015 Sensitivity of an intense rain event between atmosphere-only and atmosphere-ocean regional coupled models: 1996 *Q. J. R. Meteorol. Soc.* **141** 258–71

Blanchet J, Molinié G and Touati J 2018 Spatial analysis of trend in extreme daily rainfall in southern France *Clim. Dyn* **51** 799–812

Caillaud C 2019 *METEO-FRANCE, RADAR COMEPHORE Hourly Precipitation Amount Composite* (Aeris) (https://doi.org/10.25326/360)

Caillaud C, Somot S, Alias A, Bernard-Bouissières I, Fumière Q, Laurantin O, Seity Y and Ducrocq V 2021 Modelling Mediterranean heavy precipitation events at climate scale: an object-oriented evaluation of the CNRM-AROME convection-permitting regional climate model *Clim. Dyn.* **56** 1717–52

Champeaux J-L, Dupuy P, Laurantin O, Soulan I, Tabary P and Soubeyroux J-M 2009 Les mesures de précipitations et l'estimation des lames d'eau à Météo-France: état de l'art et perspectives *Houille Blanche* **95** 28–34

Chochon R, Martin N, Lebourg T and Vidal M 2021 Analysis of extreme precipitation during the mediterranean event associated with the Alex storm in the Alpes-Maritimes: atmospheric mechanisms and resulting rainfall *SimHydro 2021: Models for complex and global water issues* (*Sophia-Antipolis, France*) (available at: https://hal.science/hal-03374712v2)

Dayan U, Nissen K and Ulbrich U 2015 Review article: atmospheric conditions inducing extreme precipitation over the eastern and western Mediterranean *Nat. Hazards Earth Syst. Sci.* **15** 2525–44

De Zolt S, Lionello P, Nuhu A and Tomasin A 2006 The disastrous storm of 4 November 1966 on Italy *Nat. Hazards Earth Syst. Sci.* **6** 861–79

Drobinski P *et al* 2018 Scaling precipitation extremes with temperature in the Mediterranean: past climate assessment and projection in anthropogenic scenarios *Clim. Dyn.* **51** 1237–57

Drobinski P, Alonzo B, Bastin S, Da Silva N and Muller C 2016 Scaling of precipitation extremes with temperature in the French Mediterranean region: what explains the hook shape? *J. Geophys. Res. Atmos.* **121** 3100–19

Ducrocq V *et al* 2014 HyMeX-SOP1. The field campaign dedicated to heavy precipitation and flash flooding in the northwestern Mediterranean *Bull. Am. Meteorol. Soc.* **95** 1083–100

Fumière Q, Déqué M, Nuissier O, Somot S, Alias A, Caillaud C, Laurantin O and Seity Y 2020 Extreme rainfall in Mediterranean France during the fall: added value of the CNRM-AROME convection-permitting regional climate model *Clim. Dyn.* **55** 77–91

Ginesta M, Yiou P, Messori G and Faranda D 2023 A methodology for attributing severe extratropical cyclones to climate change based on reanalysis data: the case study of storm Alex 2020 *Clim. Dyn.* **61** 229–53

Hersbach H *et al* 2020 *Q. J. R. Meteorol. Soc.* **146** 1999–2049

Hersbach H *et al* 2023 ERA5 hourly data on single levels from 1940 to present. copernicus climate change service (C3S) climate data store (CDS) (https://doi.org/10.24381/cds.adbb2d47)

Jansa A *et al* 2014 MEDEX: a general overview *Nat. Hazards Earth Syst. Sci.* **14** 1965–84

Kreitz M 2021 Trois phénomènes météorologiques exceptionnels durant l'automne 2020 *La Météorologie* **112** 115–24

Lavers D A, Simmons A, Vamborg F and Rodwell M J 2022 An evaluation of ERA5 precipitation for climate monitoring *Q. J. R. Meteorol. Soc.* **148** 3124–37

Lebeaupin Brossier C, Drobinski P, Béranger K, Bastin S and Orain F 2013 Ocean memory effect on the dynamics of coastal heavy precipitation preceded by a mistral event in the northwestern Mediterranean *Q. J. R. Meteorol. Soc.* **139** 1583–97

Lebeaupin C, Ducrocq V and Giordani H 2006 Sensitivity of torrential rain events to the sea surface temperature based on high-resolution numerical forecasts *J. Geophys. Res.* **111** D12110

Meredith E P, Semenov V A, Maraun D, Park W and Chernokulsky A V 2015 Crucial role of Black Sea warming in amplifying the 2012 Krymsk precipitation extreme *Nat. Geosci.* **8** 615–9

Meroni A N, Parodi A and Pasquero C 2018 Role of SST patterns on surface wind modulation of a heavy midlatitude precipitation event *J. Geophys. Res. Atmos.* **123** 9081–96

Nuissier O, Ducrocq V, Ricard D, Lebeaupin C and Anquetin S 2008 A numerical study of three catastrophic precipitating events over southern France. I: numerical framework and synoptic ingredients *Q. J. R. Meteorol. Soc.* **134** 111–30

Pastor F, Estrela M J, Narrocha D P and Milln M M 2001 Torrential rains on the Spanish Mediterranean coast: modeling the effects of the sea surface temperature *J. Appl. Meteorol.* **40** 1180–95

Ribes A, Thao S, Vautard R, Dubuisson B, Somot S, Colin J, Planton S and Soubeyroux J-M 2019 Observed increase in extreme daily rainfall in the French Mediterranean *Clim. Dyn.* **52** 1095–114

Rivoire P, Martius O and Naveau P 2021 A comparison of moderate and extreme ERA-5 daily precipitation with two observational data sets *Earth Space Sci.* **8** e2020EA001633

Stocchi P and Davolio S 2016 Intense air-sea exchange and heavy rainfall: impact of the northern Adriatic SST *Adv. Sci. Res.* **13** 7–12

Tabary P, Dupuy P, Lhenaff G, Gueguen C, Moulin L, Laurantin O, Merlier C and Soubeyroux J M 2012 A 10-year (1997–2006) reanalysis of Quantitative Precipitation Estimation over France: methodology and first results *Weather Radar and Hydrology, Proc. Symp.* (*Exeter, UK*, *April 2011*) vol 351 (International Association of Hydrological Sciences, Publ) pp 255–60

Terray L 2021 A dynamical adjustment perspective on extreme event attribution *Weather Clim. Dyn.* **2** 971–89

Terray L 2023 A storyline approach to the June 2021 Northwestern North American Heatwave *Geophys. Res. Lett.* **50** e2022GL101640

Van den Dool H M, Huang J and Fan Y 2003 Performance and analysis of the constructed analogue method applied to U.S. soil moisture over 1981–2001 *J. Geophys. Res.* **108** 8617